ELSEVIER

Journal of Alloys and Compounds 401 (2005) 178–183

Journal of ALLOYS AND COMPOUNDS

www.elsevier.com/locate/jallcom

Iron and other elements studies in cancerous and non-cancerous prostate tissues

W.M. Kwiatek [a,*], A. Banaś [a,b], K. Banaś [a], M. Gajda [c], M. Gałka [d], G. Falkenberg [e], T. Cichocki [c]

[a] *Institute of Nuclear Physics, Polish Academy of Sciences, ul. Radzikowskiego 152, 31-342 Kraków, Poland*
[b] *Institute of Physics, Jagiellonian University, Reymonta 4, 30-059 Kraków, Poland*
[c] *Department of Histology, Collegium Medicum, Jagiellonian University, Kopernika 7, 31-034 Kraków, Poland*
[d] *Gabriel Narutowicz Hospital, Prądnicka 37, 31-202 Kraków, Poland*
[e] *Hasylab, DESY Notkestraße 85, D-22603 Hamburg, Germany*

Received 6 December 2004; received in revised form 13 February 2005; accepted 3 March 2005
Available online 15 June 2005

Abstract

To understand the role of trace elements in the oxidative stress, which may be an important factor in the pathogenesis of prostate cancer, we investigated the distribution and chemical state of Fe using synchrotron radiation. Therefore, both synchrotron radiation induced X-ray emission (SRIXE) and X-ray absorption near-edge structure (XANES) techniques have been applied to study cancerous and non-cancerous prostate tissues.

The results obtained in this work prove that SRIXE and XANES techniques are complementary ones for analysis of trace elements in biomedical samples. The absorption K-edge position of iron determined in cancerous tissue is shifted by 2.9 eV towards higher energies in comparison to iron absorption K-edge determined in non-cancerous tissue. The information obtained in this way may help to understand the role of oxidation state of iron in the oxidative stress underlying the oncogenesis.

Keywords: Prostate; Oxidation state; Iron; X-ray spectroscopy; Synchrotron radiation

1. Introduction

The interest for free radicals (and oxidative stress derived from free radical-generating processes) has been greatly increased during the last decades, due to their proposed involvement in more than 100 physiological and pathological conditions, including aging and carcinogenesis [1]. Free radicals are extremely reactive and because they are generated in the intracellular space, they are able to damage or/and modify all cellular constituents. It is well known that low levels of free radicals and other reactive oxygen species (ROS) are continuously present in cells under physiological conditions and cellular redox state is precisely regulated. When the rate of generation of ROS increases and the defense capacity of the cell is surpassed, the toxic effects of ROS appear [2].

Many different evidences indicate that various metals act as catalysts in the oxidative damage of biological macromolecules, and therefore, the toxicity associated with these metals may be due, at least in part, to their ability to generate free radicals [3–5]. Recent studies have shown that toxic effects of such metals as Fe, Cu, Cr, Ni, Cd, V depend on ROS generation. Specific differences in the toxicity of various metals may come from differences in their transport, chemical reactivity, solubility and the formation of complexes within the cell, but the general mechanisms [6–8] involved in the metal-associated formation of free radicals are generally the same.

Human body contains 3–4 g of iron, 60% of which is associated with hemoglobin. The remaining iron is generally

* Corresponding author. Tel.: +48 12 66 28 235; fax: +48 12 66 28 423.
E-mail address: wojciech.kwiatek@ifj.edu.pl (W.M. Kwiatek).

0925-8388/$ – see front matter © 2005 Elsevier B.V. All rights reserved.
doi:10.1016/j.jallcom.2005.03.090

stored in the cells in ferritin or transported by transferrin in the form of Fe (III) [9]. It is released from ferritin when required for incorporation in the iron-containing proteins and only a small part of it is found as low molecular weight, redox active and chelate fraction. In cells, iron is in constant transition between ferritin, the 'low molecular weight pool' and iron-containing functional proteins. Under certain pathological conditions, the intracellular pool of redox active iron is increased [1]. It is well known that $O_2^{\bullet}$ and other biological electron donors can reduce Fe(III) to Fe(II) in ferritin and iron–sulphur centers thereby making it readily released [10]. Additionally, H_2O_2 and lipid peroxides may oxidize the iron in heme-containing proteins also facilitating its release [11,12]. It is obvious that cells have to control precisely the levels of $O_2^{\bullet}$ and peroxides in order to avoid metal catalyzed production of free radicals. Otherwise, Fenton reaction may take place (Eqs. (1) and (2)).

$$Fe^{2+} + H_2O_2 \rightarrow Fe^{3+} + {}^{\bullet}OH + OH^{-} \quad (1)$$

$$Fe^{3+} + O_2^{\bullet -} \rightarrow Fe^{2+} + O_2 \quad (2)$$

The sum of these reactions represents the reaction described by Haber and Weiss in early 1930s (Eq. (3)).

$$H_2O_2 + O_2^{\bullet -} \rightarrow O_2 + {}^{\bullet}OH + OH^{-} \quad (3)$$

Metals other than Fe, i.e. Cu, Cr, Ni, Co, Ti, V may also catalyze this type of reaction in vitro leading to the formation of the extremely reactive hydroxyl radical. The precise role of iron in potentiating carcinogenesis is not clear so far. However, because free radicals are generally believed to play a central role in cell transformation, and as iron facilitates the formation of ROS, the iron may act as carcinogenesis promoter [13,14].

In this paper we decided to:

(1) investigate the distributions of some elements, which may be suspected to take part in oncogenesis and
(2) determine proper oxidation state of iron in cancerous and non-cancerous prostate tissues.

All analyses were carried out by using synchrotron radiation.

Synchrotron is an ideal X-ray source, which can provide an extremely high brilliance (high intense photon) and tunable (energy variability) synchrotron radiation (SR), to investigate trace metallic elements contained in biological samples. Synchrotron radiation induced X-ray emission (SRIXE) and X-ray absorption near-edge structure (XANES) spectroscopy [15] with a SR microbeam are two highly useful techniques: SRIXE determines existence and distribution of trace elements in a single cell and XANES spectroscopy provides information about electronic structure and the binding configuration of the probing element.

2. Materials and methods

The samples were gained after surgery: radical removal of prostate due to the cancer from six patients. As a control group, healthy prostates were taken from two patients operated for urinary bladder cancer. Just after the prostate removal, within half of an hour, samples were mounted on metal holders and immediately frozen in liquid nitrogen. The frozen samples were cut into 14 μm thick sections on a cryomicrotome and placed on 2.5 μm thick Mylar foil. Adjacent sections were mounted on poly-l-lysine coated slides, stained routinely and examined histologically. All samples underwent the same preparation and storage procedures.

All sections were divided into groups: cancerous with appropriate Gleason score and healthy. Histopathological typing using the Gleason system (five grades based on glandular patterns and degree of differentiation) is the most universally accepted tool for evaluation of tumor aggressiveness.

After the measurements, the sections irradiated with synchrotron radiation were stained for enabling a proper histological classification of the measured areas.

In this study, the measurements by SRIXE and XANES spectroscopy were carried out on the L-beamline at the Hasylab, DESY (Germany). The microprobe setup at the beamline L, described by the authors in this issue of the journal, is a powerful tool for simultaneous multi-element trace analysis of microsamples. Using the highly brilliant synchrotron source with its white and linearly polarized radiation for fluorescence excitation it is routinely possible to detect the elements with atomic numbers between 13 and 92 with minimum detection limits c_{MDL} of down to 0.1 pg/μg [16]. During the experiments the 2-dimensional (2D) scans were made on selected areas on prepared tissues samples in order to obtain distributions of various trace elements and to perform the quality analysis of selected areas in the samples. Typical X-ray fluorescence spectrum with the monochromatic synchrotron radiation beam of 17 keV was taken from each

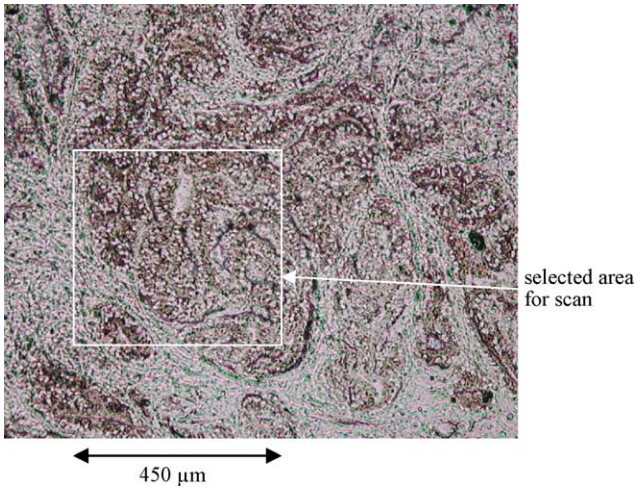

Fig. 1. Histological view of cancerous prostate tissue with selected area for scan (450 μm × 450 μm).

spot of pre-selected area. The distribution image (mapping) of certain element were obtained by detailed analysis of each spectrum:

(1) Background deduction and normalization to storage ring beam current since the experimental set-up and conditions for all samples remained the same (there was linear proportion between irradiated photons on the sample and beam current);
(2) integration of the area under the peak of Kα corresponding to chosen element (e.g. Fe) over the region of interest (ROI) (these procedure was repeated for each spot);
(3) construction of square matrix composed of the numbers equal to areas (see point 2);
(4) visualization of the matrix by using Mathcad 8.0 [17].

The 2D scans were acquired for 25 s/pixel with a 15 μm step in the *X* and *Y* directions. Typical scans were about 450 μm × 450 μm.

The K-edge XANES measurements were performed in fluorescence mode by measuring the X-ray fluorescence line of 6.4 keV that corresponds to Fe Kα line. The white synchrotron radiation beam was monochromatized and the monochromatic beam was scanned in the photon energy

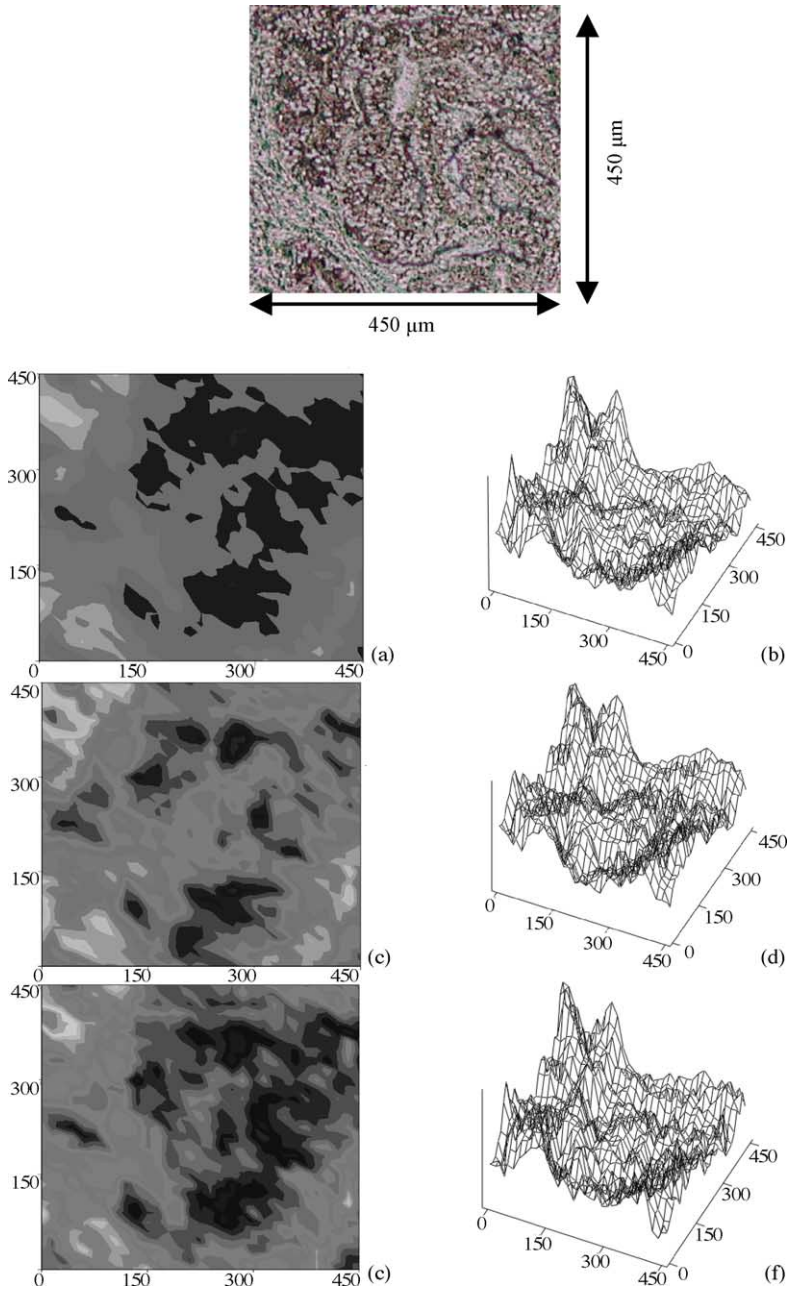

Fig. 2. Distribution of Cl (a, 2D; b, 3D), K (c, 2D; d, 3D), S (e, 2D; f, 3D) in the selected area of scan shown at the top figure. Where 2D stands for two-dimensional plot and 3D for three-dimensional plot.

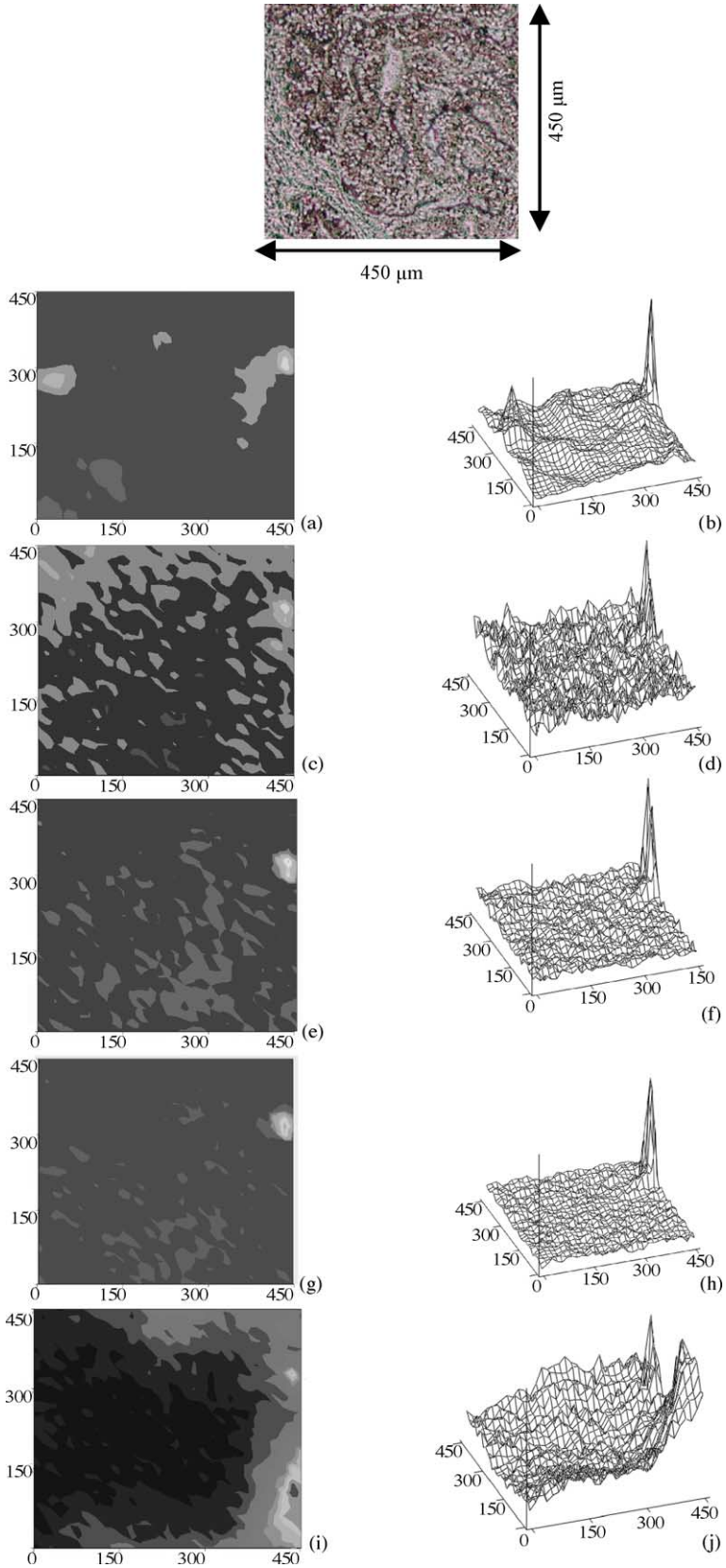

Fig. 3. Distribution of Fe (a, 2D; b, 3D), Mn (c, 2D; d, 3D), Cr (e, 2D; f, 3D), Ni (g, 2D; h, 3D), Cu (i, 2D; j, 3D) in the selected area of scan shown at the top figure. Where 2D stands for two-dimensional plot and 3D for three-dimensional plot.

range from 7090 to 7150 eV with 0.2 eV or 2 eV steps and then set to 7.112 keV, Selected minerals, such as Fe_2O_3 and $(FeMg)SiO_3$, were chosen as standards for an appropriate oxidation state of iron (Fe(III) and Fe(II), respectively). Iron XANES spectra were collected from about 22 eV below to 38 eV above the absorption edge for metallic iron so called Fe(0) (the absorption edge is at 7112 eV). The energy step increments of 2.0, 0.2 and 2.0 eV over the ranges: −22 to −2, −2 to 18 and 18–38 eV above the iron absorption edge, respectively. The acquisition time for tissue samples was 30 s per energy step, while for standards 2 s. The beam size for SRIXE and XANES analysis was about 16 μm × 14 μm.

3. Results

The results obtained reveal the different spatial distributions of the constituent elements in a tissue. Fig. 1 shows an example of histological picture of cancer prostate tissue (classified as CA with Gleason score 5).

The distributions for elements, such as Cl, K, S, correspond to the tissue structure. Other elements show more random localization. Elemental distribution of Cl, K and S in the selected area for scan marked in Fig. 1 are presented in Fig. 2.

The elemental distribution of Fe, Mn, Cu and Ni in the investigated region is shown in Fig. 3. In order to be able to compare presented results in Figs. 2 and 3 the elemental distribution presents normalized counts per μm^2. As one can see there are areas with high concentrated ions of these elements that indicate positive correlation of their localization. Due to careful histological investigation of that area during the measurements and afterwards the case of possible contamination has been excluded.

Special attention was paid to Fe distribution. Areas of higher concentration of iron were chosen to perform XANES analysis to evaluate iron oxidation state. Always the same histological structure was taken into account while analyzing the data. In order to establish the relation between iron oxidation state and iron absorption K-edge position the XANES spectra of standards were obtained. As shown in Fig. 4, the absorption characteristic curves for Fe(III) in Fe_2O_3 and Fe(II) in $(FeMg)SiO_3$ are shifted to what confirms our previous results [18] and enables the evaluation of iron K-edge position for different iron oxidation state in tissues.

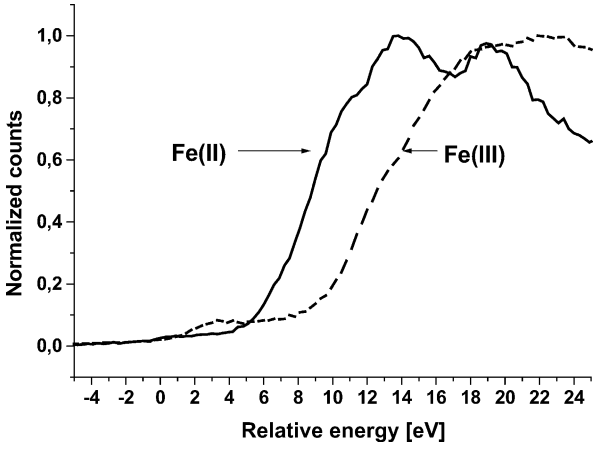

Fig. 4. Iron XANES spectra measured in standards.

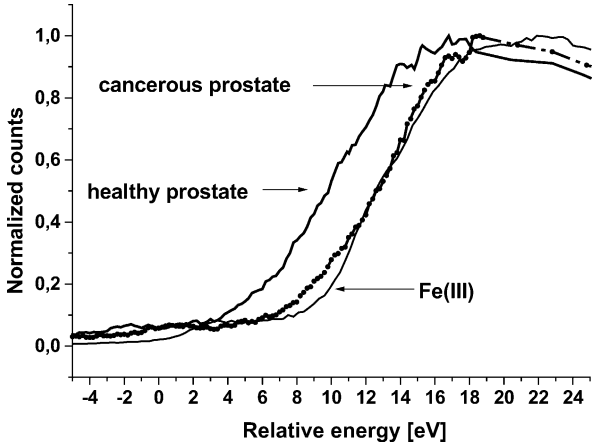

Fig. 5. Iron XANES spectra from places containing high iron concentration in the cancerous and healthy prostate tissues compared to XANES spectrum of Fe(III).

The K-edge XANES spectra were normalized to maximum counts and storage ring beam current. The "zero level" of the XANES spectra were found by subtracting the background as a straight line fitted to the XANES spectrum data below pre-edge peak positions. The energy scale was set to 0 eV for iron absorption K-edge determined for metallic iron (Fe(0)). The example of the spectra obtained for healthy and cancerous tissues are shown in Fig. 5. The XANES spectra were measured at several points in the scanned area (healthy or cancerous) and then after normalization they were averaged in order to improve statistics for better comparison. In each point three spectra were taken. And once again it should be pointed out that during the analysis and averaging process the same histological structures were taken into account.

In order to precisely find the energy distance between absorption K-edge position for iron in healthy and cancerous

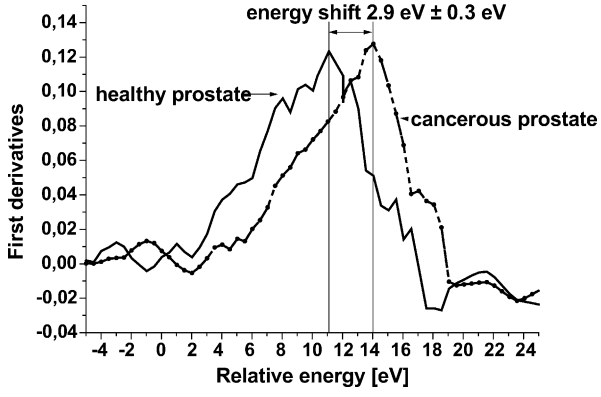

Fig. 6. First derivatives of XANES spectra taken from cancerous and healthy tissues shown in Fig. 5.

tissues first derivatives were calculated. The first derivatives of each spectrum were obtained using a Savitzky–Golay algorithm. Fig. 6 shows results of this calculation. As one can see the energy shift of 2.9 eV toward higher energies has been found for iron K-edge absorption determined for cancerous samples.

4. Discussion

The different patterns of trace elements localization and/or concentration may result from:

- type of tissues present in measured area (tissue dependent elements concentration) and
- changes in tissues content as well as intercellular changes resulting from cancerous process.

As Fe, Cu, Ni, Mn and Cr are suspected to be involved in the process of carcinogenesis [1,9] we looked for their concentration levels by making 2D mapping (the example is shown in Fig. 3). The figure shows that the metals show high peak of concentration in the same restricted area. The fact that high Fe concentration we have found also in other peak without co-localization of other above mentioned elements may point to the following conclusions:

- First, we dealt with crystals.
- Second, the diversion of crystal compositions speaks against assumption that contamination was measured.

Besides the crystallites, iron shows specific pattern of concentration. It forms low linear maxima reflecting probably concentration of hemoglobin (blood vessels accumulation).

Hem-iron is one of the main sources of free radical formation. This might be confirmed by Fe(II)/Fe(III) balance shown in Figs. 5 and 6.

It seems that 2D mapping together with XANES analysis may be a useful tool for further research on the process of carcinogenesis.

A synchrotron radiation microbeam with high brilliance made it possible to analyze very low concentrations of trace elements at the cellular level without isolating or purifying procedures. Because nutrition and metabolism alteration have influence on trace elements level their concentration can be an important indicator in other than cancer diseases. Moreover, a study of the interactions between toxic and essential elements is an approach to elucidate the metal promoted toxicity and perhaps in future also their protective role.

Acknowledgements

The authors wish to thank Prof. Jerzy Stachura and Dr. Grzegorz Dyduch from Collegium Medicum at the Jagiellonian University for their assistance in tissue samples classification. This work has been supported by HASYLAB, DESY, Hamburg, Germany, under project II-02-010, the IHP-Contract HPRI-CT-1999-00040/2001-00140 of the European Commission.

References

[1] D. Galaris, A. Evangelou, Crit. Rev. Oncol. Hematol. 42 (2002) 93–103.
[2] B. Halliwell, J.M.C. Gutteridge, Free Radicals in Biology and Medicine, third ed., Oxford University Press, New York, 1999.
[3] S.J. Stohs, D. Bagchi, Free Radic. Biol. Med. 18 (1995) 321–336.
[4] S.I. Liochev, I. Fridovich, IUBMB Life 48 (1999) 157–161.
[5] J. Termini, Mutat. Res. 450 (1–2) (2000) 107–124.
[6] F. Okada, Redox Report 7 (6) (2002) 357–368.
[7] L. Benov, Protoplasma 217 (1–3) (2001) 33–36.
[8] K. Keyer, A.G. Strohmeier, J.A. Imlay, J. Bact. 177 (23) (1995) 6782–6790.
[9] M.C.R. Symons, J.M.C. Gutteridge, Free Radicals and Iron: Chemistry, Biology, and Medicine, Oxford Science Publications, Oxford, 1998.
[10] K.J.A. Davies, IUBMB Life 50 (2000) 279–289.
[11] D. Galaris, E. Cadenas, P. Hochstein, Free Radic. Biol. Med. 6 (5) (1989) 473–478.
[12] D. Galaris, L. Eddy, A. Arduini, E. Cadenas, P. Hochstein, Biochem. Biophys. Res. Commun. 160 (1989) 1162–1168.
[13] V. Abalea, J. Cillard, M.P. Dubos, J.P. Anger, P. Cillard, I. Morel, Carcinogenesis 19 (6) (1998) 1053–1059.
[14] S. Toyokuni, Free Radic. Biol. Med. 20 (4) (1996) 553–566.
[15] A. Bianconi, in: D.C. Koningsberger, R. Prins (Eds.), X-ray Absorption: Principles, Applications, Techniques of EXAFS, SEXAFS and XANES, Wiley and Sons, New York, 1988 (Chapter 11).
[16] G. Falkenberg, O. Clauss, A. Swiderski, Th. Tschentscher, X-ray Spectrom. 30 (2001) 170–173.
[17] Mathcad 8.0, www.mathcad.com.
[18] W.M. Kwiatek, A.L. Hanson, C. Paluszkiewicz, M. Gałka, M. Gajda, T. Cichocki, J. Alloys Comp. 362 (2004) 83–87.